Chinese Chemical Letters 34 (2023) 107312

Contents lists available at ScienceDirect

Chinese Chemical Letters

journal homepage: www.elsevier.com/locate/cclet

Soft carbon-coated bulk graphite for improved potassium ion storage

Xiaqing Chang, Ning Sun*, Huanyu Zhou, Razium A. Soomro, Bin Xu*

State Key Laboratory of Organic-Inorganic Composites, Beijing Key Laboratory of Electrochemical Process and Technology for Materials, Beijing University of Chemical Technology, Beijing 100029, China

ARTICLE INFO

Article history:
Received 13 January 2022
Revised 23 February 2022
Accepted 10 March 2022
Available online 13 March 2022

Keywords:
Graphite
PTCDA
Potassium-ion battery
Anode materials
Carbon coating

ABSTRACT

Potassium-ion batteries (PIBs) have attracted tremendous attention for large-scale energy storage fields based on abundant potassium resources. Graphite is a promising anode material for PIBs due to its low potassium ion intercalation voltage and mature industrialized preparation technology. However, the inability of graphitic structures to endure large volume change during charge/discharge cycles is a major limitation in their advancement for practical PIBs. Herein, a soft carbon-coated bulk graphite composite is synthesized using PTCDA as a carbon precursor. The PTCDA-derived soft carbon coating layer with large interlayer distance facilities fast potassium ion intercalation/extraction in the BG@C composite and buffers severe volume change during the charge/discharge cycles. When tested as anode for PIBs, the composite realizes enhanced rate capability (131.3 mAh/g at 2 C, 1 C = 279 mA/g) and cycling performance (capacity retention of 76.1% after 150 cycles at 0.5 C). In general, the surface modification route to engineer graphite anode could inherently improve the electrochemical performance without any structural alteration.

Lithium-ion batteries (LIBs) have been widely used in portable electronics, power tools and electric vehicle due to their high energy density, high power density and long cycle life. However, in the realm of large-scale energy storage, LIBs are hampered by a lack of lithium-resource availability and the rising costs [1–4]. Herein, sodium-ion batteries (SIBs) and potassium-ion batteries (PIBs) have gotten a lot of interests as LIB alternatives based on their accessible materials and chemical features comparable to lithium [5,6]. In comparison, PIBs offer a lower K^+/K standard potential (−2.93 V *vs.* SHE) than Na^+/Na (−2.71 V *vs.* SHE), realizing a greater full-cell operating voltage and consequently a higher energy density. In addition, the smaller solvated K^+ attributed to the lower charge density of K^+ facilities fast ionic transport and provides a high power density [7–9]. Therefore, PIBs are regarded as a promising technology for large-scale energy storage.

Ji and coworkers demonstrated the reversible electrochemical potassiation/depotassiation of K^+ in graphite, making a breakthrough in PIBs' development [10]. Since then, engineering a superior PIBs-based electrode has become a hotspot in materials research. Graphite, as a commercial anode of LIBs, is a preferred material for PIBs based on its low-cost and low intercalation voltage of ~0.2 V. In the case of graphite, K ion storage is based on intercalation/deintercalation mechanism allowing a theoretical capacity of 279 mAh/g, corresponding to the graphite intercalation compound of KC_8 [11–13]. Despite K ions affinity for graphite, their large ionic radius (1.33 Å) makes its intercalation challenging. Furthermore, the intercalation process causes a 60% volume expansion and massive distortion of the graphite structure [14–17]. As a result, graphite as an anode for PIBs shows poor cycling performance and rate capability.

Strategies such as forming a stable solid electrode interface (SEI) *via* optimized electrolyte systems [18–21], adjusting the interlayer distance [22–24], and surface modification of graphite [25–27] have been adopted to overcome these challenges. In the case of the surface coating of graphite, effective volume buffering during the intercalation/deintercalation process could be anticipated, which could enhance the cycle stability and rate capability of the electrode. Feng *et al.* utilized atomic layer deposition to coat the atomic layer of Al_2O_3 on graphite. The Al_2O_3 coating layer enabled the formation of a robust SEI layer and thus improved the cycling performance of the electrode to 233 mAh/g after 50 cycles at a current density of 0.05 A/g, which is much superior to the pristine natural graphite (92 mAh/g) [28]. Here, carbon materials with high electronic conductivity could be a better choice for coating the surface of graphite. Han *et al.* synthesized a polyvinylidene fluoride (PVDF) derived F-doped carbon-coated natural microcrystalline graphite (NMG) composite *via* a scalable solution reflux process and thermal annealing. The carbon coating could effectively suppress the volume change along graphite's c-axis, allowing improved K ion diffusion kinetics. Thus, the composite

* Corresponding authors.
E-mail addresses: ningsun@mail.buct.edu.cn (N. Sun), xubin@mail.buct.edu.cn (B. Xu).

https://doi.org/10.1016/j.cclet.2022.03.035
1001-8417/

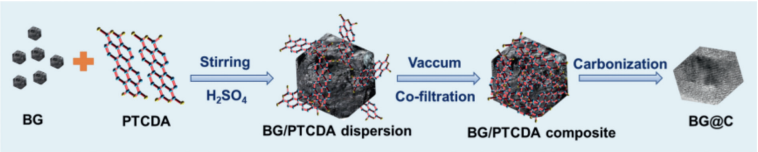

Fig. 1. The preparation of PTCDA-derived soft carbon-coated bulk graphite (BG@C).

realized a specific capacity of 191 mAh/g after 120 cycles at 0.1 A/g with a capacity retention of 74.3% [29]. Nan *et al.* prepared a N-doped carbon nanosheet coated multilayer graphite using urea as a nitrogen-containing carbon source. The composite realized improved specific capacity, cycle durability, and rate capability with a capacity retention of 97.5% after 1000 cycles at 0.2 A/g [30]. Thus, surface engineering of graphite could be a viable route to improve the inherent electrochemical performance of PIBs anode without any structural alteration.

3,4,9,10-Perylene tetracarboxylic dianhydride (PTCDA), a typical conjugated carbonyl compound, is a common soft carbon precursor [31–33]. The soft carbon often has a higher electronic conductivity and less defect compared to hard carbon and thus could serve as a suitable surface modifier for graphite. Herein, PTCDA-derived soft carbon-coated bulk graphite composite (BG@C) is proposed as an efficient anode for PIBs. The bulk graphite material is homogenized with PTCDA in concentrated sulfuric acid (H_2SO_4, 98%) followed by carbonization to convert the PTCDA to carbon layers. The BG@C based on its soft carbon-coated surface, realizes superior intercalation/de-intercalation property of K^+ with high volume expansion endurance. The composite demonstrates a high reversible specific capacity of 232.8 mAh/g in the first cycle with a capacity retention of ~76.1% after 150 cycles at 0.5 C, superior to the bulk graphite (BG) with a charge specific capacity of 211.3 mAh/g and capacity retention of ~31.4% at same conditions. In addition, the BG@C delivers a higher reversible capacity of 131.1 and 46.1 mAh/g at 2 and 5 C, respectively. In general, the PTCDA-derived soft carbon coating is an effective route to realize efficient graphite-based PIBs anode.

Fig. 1 illustrates the fabrication process of PTCDA-derived soft carbon-coated bulk graphite (BG@C) composite. In a typical experiment, PTCDA was first dispersed in the concentrated H_2SO_4 (98%) to form a homogeneous pink solution. PTCDA with the polycyclic aromatic framework can be protonated and completely homogenized using concentrated H_2SO_4 [34]. The bulk graphite was then added under magnetic stirring and continued for 2 h allowing the deposition of PTCDA molecules over the bulk graphite *via* noncovalent forces, including van der Waals and aromatic interactions. The suspension was then placed into cold water to absorb the massive heat generated by the rapid dilution of H_2SO_4. The precipitates were later collected by vacuum filtration and dried, followed by carbonization at 900 °C under Ar atmosphere resulting in a homogeneous soft carbon coating over bulk graphite.

FTIR analysis was carried to investigate the chemical structure of PTCDA coated bulk graphite (BG@PTCDA) in reference to pristine PTCDA. Fig. 2a shows that the standard PTCDA consists of a peak at ~1774 cm^{-1} that corresponds to the C=O bond of the carbonyl groups. The peaks at ~1594, 1301 and 1020 cm^{-1} are attributed to C=C stretching vibration, C-O and C-O-C bonds, respectively [35,36]. In the case of the BG@PTCDA, the typical peaks of PTCDA could be observed, indicating its successfully surface coating of the bulk graphite. Fig. 2b shows the XRD pattern for BG@C consisting of a sharp peak at ~26.4° and four weak peaks at ~42.2°, ~44.5°, ~54.5° and ~77.4°. The peak pattern is well-indexed to the typical graphite phase standardized against ICCD card No. 41-148725. The XRD pattern has no evidence of PTCDA justifying its complete carbonization and transformation into a thin and amorphous layer of

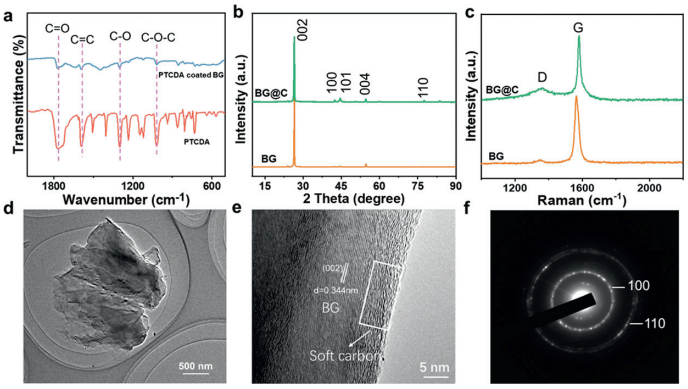

Fig. 2. Physical and chemical characteristics of the BG and BG@C samples: (a) FTIR spectra, (b) XRD patterns and (c) Raman spectra. Microstructure of the BG@C sample: (d, e) TEM images and (f) SAED pattern.

soft carbon. Fig. 2c shows the Raman analysis of BG@C consisting of typical D and G bands at 1350 and 1580 cm^{-1} corresponding to the disordered carbon and ordered graphite, respectively. The I_D/I_G ratio reflects the disorder degree of the graphite material [37] and in the case of BG@C, the ratio increases to 0.39 from 0.07 for BG. Thus, BG@C could contain more defects and has higher disorder degree based on the soft carbon layer.

The morphology and microstructure of the BG@C and BG were determined using SEM and HRTEM. Fig. S1 (Supporting information) shows that both samples have similar particle sizes of 4–11 μm, with the surface of the BG@C relatively rough compared to BG due to the pyrolysis of PTCDA into the carbon layer on the graphite surface. Fig. 2d shows the HRTEM images of the BG@C with evidence of lamellar graphitic flakes structure. Fig. S2 (Supporting information) shows the HRTEM images of the bulk graphite and PTCDA-derived soft carbon. The bulk graphite (Fig. S2a) consists of a well-ordered long-range structure with an interlayer distance of ~0.344 nm. In comparison, the PTCDA-derived soft carbon consists of a turbostratic lattice with an enlarged interlayer distance of ~0.385 nm. In the case of BG@C (Fig. 2e), a soft carbon coating with a thickness of ~6 nm is evident that could efficiently buffer structural change during the charge/discharge process. Moreover, the content of PTCDA-derived soft carbon on the surface of the bulk graphite is calculated to be 4 wt% (Fig. S3 in Supporting information), and selected area electron diffraction (SAED) comprised of bright diffraction rings confirms negligible structural alteration in bulk graphite after the carbon coating (Fig. 2f). Moreover, the BG@C has a low specific surface area of 4.8 m^2/g with a pore volume of 0.02 cm^3/g (Fig. S4 in Supporting information).

Fig. 3 shows the electrochemical potassiation profiles of BG@C electrode in reference to pristine BG electrode. The corresponding CV curves at 0.1 mV/s in the potential window of 0.01 and 3 V consist of an irreversible peak at ~0.71 V in the first cathodic scan, attributed to the decomposition of electrolyte and the formation of SEI layer on the surface of the electrode. The peak later disappears, indicating the formation of SEI in the initial cycle [38–40]. The intercalation process of K^+ into the graphite is responsible for the

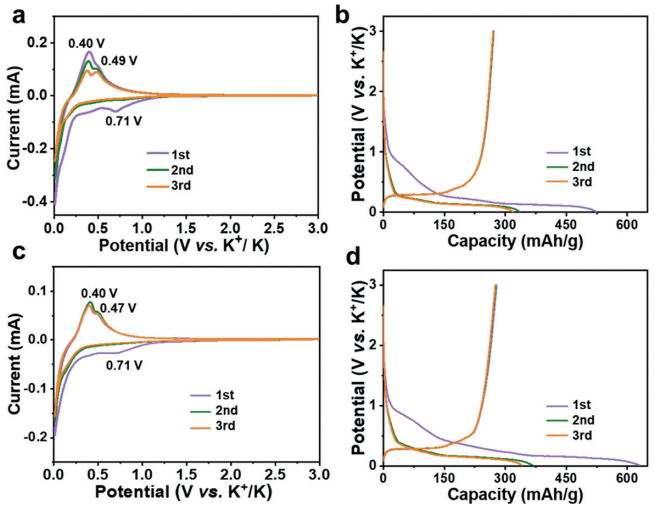

Fig. 3. Cyclic voltammograms curves at a scan rate of 0.1 mV/s and the first three charge/discharge profiles at a current density of 0.1 C of (a, b) BG and (c, d) BG@C electrodes, respectively.

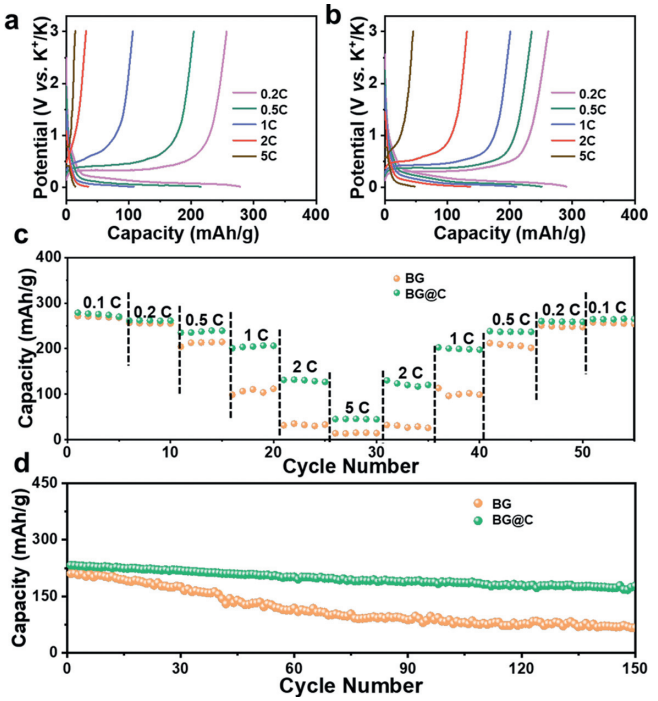

Fig. 4. The electrochemical performance of the BG@C electrode with the pristine BG electrode as a comparison. Charge/discharge profiles at various current densities of (a) BG and (b) BG@C electrodes. (c) Rate performance and (d) cycle stability at a current density of 0.5 C.

strong peak at around 0.05 V with the formation of KC_8 as a complete intercalation product leading to a theoretical specific capacity of 279 mAh/g. Here, two distinct oxidation peaks correspond to the transitions between staged K-graphite intercalation compounds for the first anodic scan. Unlike BG electrode, the CV curves of the BG@C electrode are well-overlapped after initial cycle, indicating a stable graphite host structure against the large volume change during the potassiation/depotassiation process.

Figs. 3b and d show the galvanostatic charge/discharge curves of BG@C and BG electrodes at 0.1 C (1 C = 279 mAh/g). The reaction plateaus attributed to K^+ reversible intercalation/extraction reaction are evident in both cases, with BG electrode delivering a reversible specific capacity of 271.5 mAh/g in the first cycle and an initial coulombic efficiency (ICE) of 51.8%. The BG@C electrode exhibits a higher reversible specific capacity of 278.8 mAh/g with an ICE of 44.2%. In the case of BG@C electrode, the soft carbon coating promotes an irreversible reaction of K^+ due to greater surface defects, resulting in a lower ICE [29]. The initial three charge/discharge curves of the PTCDA-derived soft carbon electrode at 0.1 C could realize a reversible specific capacity of 263.6 mAh/g with an ICE of 42.9% (Fig. S5 in Supporting information). Noticeably, the soft carbon coating layer with larger interlayer distance is conducive to the intercalation of K^+ and potentially alleviate the volume change during the charge/discharge cycles, promoting rate capability and cycling performance of the devised electrode.

Figs. 4a and b show the charge/discharge curves of BG@C and BG electrodes at different current rates in the range of 0.2–5 C. In the case of BG electrode, a voltage plateau region is observed at low current density, which gradually diminishes and disappears when the current density reaches above 2 C. In contrast, BG@C electrode owing to soft-carbon coated graphitic structure exhibits a distinct reaction plateau related to the K^+ intercalation/extraction even at a high current density of 2 C. The rate performance of BG@C electrode is shown in Fig. 4c, with BG electrode as a comparison. BG electrode delivers a high reversible specific capacity of 271.5 mAh/g at 0.1 C, which rapidly declines as the current density increases and could only retain a reversible specific capacity of 13.9 mAh/g at a high current rate of 5 C. However, the BG@C electrode exhibits a relatively superior performance with reversible specific capacities of 278.8, 206.8 and 46.1 mAh/g at increased current densities of 0.1, 1 and 5 C. The enhanced rate capability is associated with larger soft carbon interlayer distance that promotes ion transfer to the graphitic layer even at high current.

Fig. 4d shows the prolonged cycling performance of BG@C and BG electrodes at 0.5 C. The BG electrode realizes a reversible K-storage capacity of 211.3 mAh/g during the initial cycle, which later declines and remains at 66.4 mAh/g after 150 cycles with a capacity retention of ~31.4%. In contrast, BG@C electrode has a higher capacity and improved cyclability at a current density of 0.5 C (140 mA/g), which shows an initial charge capacity of 232.8 mAh/g and retains a reversible capacity of 177.2 mAh/g after 150 cycles with a relatively higher capacity retention of 76.1%. The cycling performance of BG@C electrode is also superior to some previously reported graphitie anodes, such as F-doped graphite (capacity retention of 74.6% after 100 cycles at 100 mA/g) [25] and PVDF-derived carbon-confined graphite (capacity retention of 74.3% after 120 cycles at 100 mA/g) [29]. Fig. S6 (Supporting information) shows the galvanostatic charge/discharge curves of the BG and the BG@C electrodes at 0.5 C, where a distinct charge/discharge platform is observed in the initial cycle attributed to the reversibly intercalating and extracting of K^+ from the graphitic layer. The platform in the case of BG diminishes quickly with a large charge/discharge gap as cycling increases. In the case of BG@C electrode, the stable charge/discharge profile is observed for the complete 150 cycles at 0.5 C, indicating a lower polarization and good electrochemical activity.

The kinetics of BG@C was later evaluated using electrochemical impedance spectra (EIS). The Nyquist plot comprises 3 regions consisting of an interval between the X-axis and the curve in the high frequency related to the internal resistance of the cell (Rb), a semicircle in the high-middle frequency related to the charge transfer resistance (R_{ct}) and an inclined line in the low frequency representing the Warburg resistance (Z_W) [41,42]. As shown in Fig. 5a, based on the equivalent circuit, the R_b value of the BG@C electrode is simulated to be 4.2 Ω, comparable to that of BG electrode. Furthermore, the BG@C electrode has a much lower R_{ct} value (1640 Ω)

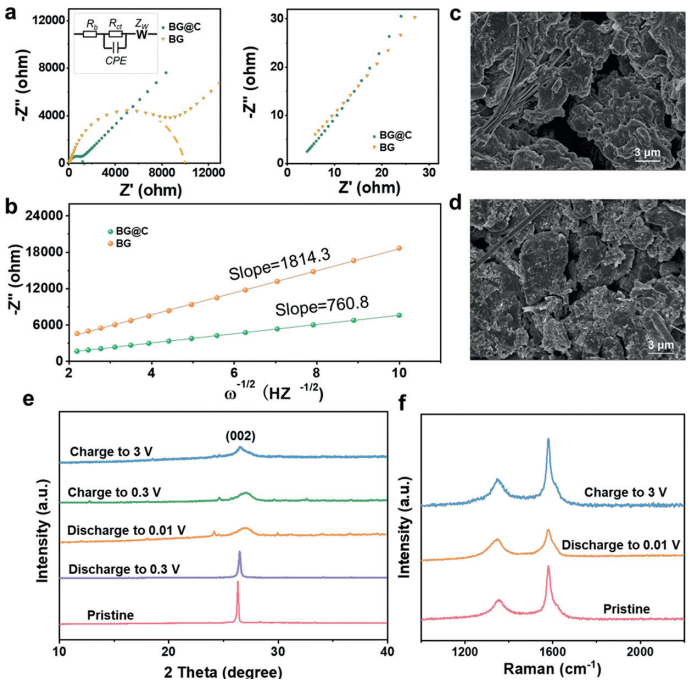

Fig. 5. (a) EIS spectra with the fitting circuit, (b) Warburg profiles of the BG and BG@C. The SEM images of (c) BG and (d) BG@C electrodes after 150 cycles at 0.5 C. (e) *Ex-situ* XRD and (f) Raman spectra of the pristine, potassiated and de-potassiated BG@C elelctrodes.

than BG electrode (~10,000 Ω), facilitating charge-transfer kinetics during the electrochemical reaction and thus realizing superior rate performance. To further explore the reason for the enhanced rate performance of BG@C electrode, the diffusion of K ion (D_{K^+}) in the BG and BG@C are calculated through the following equation [43]:

$$D_{K^+} = R^2T^2/2A^2n^2F^4C^2\sigma^2 \quad (1)$$

where R is the gas constant, T is the absolute temperature, A is the electrode surface area, n is the number of electrons per molecule during redox reaction, F is the Faraday constant, C is the K^+ concentration and σ is the Warburg factor, which can be determined *via* the linear fitting of Z′and $\omega^{-1/2}$ in the low frequency region as following:

$$Z' = R_s + R_{ct} + \sigma\omega^{-1/2} \quad (2)$$

The σ values of the BG and BG@C electrodes are 1814.3 Ω $S^{-1/2}$ and 760.8 Ω $S^{-1/2}$, respectively, as shown in Fig. 5b. According to the Eq. 1, the D_{K^+} value of BG@C electrode is 4.01×10^{-13} cm^2/s, higher than 1.02×10^{-13} cm^2/s of BG electrode, suggesting the faster K ion transportation kinetics in the BG@C electrode, which could boost the potassium ion storage performance.

The morphological evaluation of BG@C and BG was investigated using SEM after 150 cycles at 0.5 C. Fig. S7 (Supporting information) confirms the excellent structural integrity for both electrodes before the cyclization. In the case of BG electrode, cracked surface and significant structural deformation are observed post cyclization (Fig. 5c), which could be attributed to the unstable SEI film [44]. In contrast, the BG@C electrode displays a stable surface with no distinct crack (Fig. 5d), suggesting that the carbon coating layer has efficiently alleviated the graphite's c-axis volume change during the potassiation/depotassiation process. The electrochemical kinetics of the cycling process was studied by analyzing the EIS spectra of the BG@C electrode after several cycles at 0.5 C. Fig. S8 (Supporting information) shows that R_{ct} value of the BG@C electrode is 1640, 1338, 1586 and 3080 Ω after 1, 3, 10 and 50 cycles, respectively. The decline R_{ct} value after the first cycle could be attributed to the activation process of electrode [45].

Ex-situ XRD and Raman spectroscopy were carried out to reveal the structural variation of BG@C during charge/discharge process. Fig. 5e presents the *ex-situ* XRD of BG@C electrode at different charge-discharge states in the initial cycle. The (002) peak becomes broaden during discharge process and two weak peaks at 24.1° and 29.8° appeared when discharged to 0.01 V, indicating the formation of graphite intercalation compound. During charge process, the (002) peak gets gradually sharp, due to the extraction of K^+. In the Raman spectrum (Fig. 5f), the I_D/I_G value increases from 0.68 of pristine electrode to 1.30 of discharged electrode and recovers to 0.70 as charges to 3 V, which further demonstrates the good structural reversibility of BG@C electrode and favors an enhanced electrochemical performance.

In summary, PTCDA-derived soft carbon-coated bulk graphite composite (BG@C) was prepared with the assistance of concentrated H_2SO_4. The soft carbon coating layer can effectively alleviate the volume expansion of graphite electrode during the cycling process and facilitate the formation of a high-quality SEI film. Moreover, the soft carbon coating layer with large interlayer distance evidently improves the K ion diffusion kinetics, allowing the BG@C to exhibit good rate performance and cycle durability. The capacity retention improves from 31.4% to 71.6% compared with un-coated graphite electrode at 0.5 C after 150 cycles. This work provides an effective way to construct a suitable carbon coating layer on the surface of the bulk graphite for stable potassium storage.

Declaration of competing interest

The authors declare that they have no known competing financial interests or personal relationships that could have appeared to influence the work reported in this paper.

Acknowledgments

This work was financially supported by the National Natural Science Foundation of China (NSFC, Nos. 52072021, 22005023), and the Fundamental Research Funds for the Central Universities (No. buctrc202141).

Supplementary materials

Supplementary material associated with this article can be found, in the online version, at doi:10.1016/j.cclet.2022.03.035.

References

[1] L. Zhang, W. Wang, S. Lu, et al., Adv. Energy Mater. 11 (2021) 2003640.
[2] X. Li, J. Li, L. Ma, et al., Energy Environ. Mater. (2021) 1–12.
[3] X. Wu, D.P. Leonard, X. Ji, Chem. Mater. 29 (2017) 5031–5042.
[4] Y. Zhang, J. Wang, S.N. Riduan, J. Mater. Chem. A 4 (2016) 14902–14914.
[5] M. Sha, L. Liu, H.P. Zhao, et al., Carbon Energy 2 (2020) 350–369.
[6] L.B. Wang, Y.X. Ni, X.S. Hou, et al., Angew. Chem. Int. Ed. 59 (2020) 22126–22131.
[7] B. Wang, Y. Peng, F. Yuan, et al., J. Power Sources 484 (2021) 229244–229262.
[8] A. Eftekhari, Z. Jian, X. Ji, ACS Appl. Mater. Interfaces 9 (2017) 4404–4419.
[9] V. A, B. John, M. Td, ACS Appl. Energy Mater. 3 (2020) 9478–9492.
[10] Z. Jian, W. Luo, X. Ji, J. Am. Chem. Soc. 137 (2015) 11566–11569.
[11] T. Hosaka, K. Kubota, A.S. Hameed, et al., Chem. Rev. 120 (2020) 6358–6466.
[12] J. Zhang, L. Lai, H. Wang, et al., Mater. Today Energy 21 (2021) 100747–100766.
[13] S.M. Ahmed, G. Suo, W.A. Wang, et al., J. Energy Chem. 62 (2021) 307–337.
[14] Z. Xing, Y. Qi, Z. Jian, et al., ACS Appl. Mater. Interfaces 9 (2017) 4343–4351.
[15] M. Carboni, A.J. Naylor, M. Valvo, et al., RSC Adv. 9 (2019) 21070–21074.
[16] L. Li, Y.T. Li, Y. Ye, et al., ACS Nano 15 (2021) 6872–6885.
[17] W.W. Hong, Y. Zhang, L. Yang, et al., Nano Energy 65 (2019) 104038.
[18] J. Zhang, Z. Cao, L. Zhou, et al., ACS Energy Lett. 5 (2020) 3124–3131.
[19] L. Wang, J. Yang, J. Li, et al., J. Power Sources 409 (2019) 24–30.
[20] L. Qin, N. Xiao, J. Zheng, et al., Adv. Energy Mater. 9 (2019) 1902618–1902625.
[21] F. Fan, R. Ma, Q. Zhang, et al., Angew. Chem. Int. Ed. 58 (2019) 10500–10505.
[22] X. Li, Y. Lei, L. Qin, et al., Carbon 172 (2021) 200–206.
[23] Y. An, H. Fei, G. Zeng, et al., J. Power Sources 378 (2018) 66–72.

[24] Z. Tai, Q. Zhang, Y. Liu, et al., Carbon 123 (2017) 54–61.
[25] Y. Zhao, L. Yang, C. Ma, et al., Energy Fuels 34 (2020) 8993–9001.
[26] S. Jiang, Y. Li, Y. Qian, et al., J. Power Sources 436 (2019) 226847–226856.
[27] M.M. Rahman, C. Hou, S. Mateti, et al., J. Power Sources 476 (2020) 228733–228742.
[28] J.F. Chen, X.D. He, D.J. Li, et al., Int. J. Energy Res. 44 (2020) 4260–4268.
[29] L. Yang, Y. Zhao, L. Cao, et al., Energy Fuels 35 (2021) 5308–5319.
[30] S. Tian, Y. Zhang, C. Yang, et al., Electrochim. Acta 380 (2021) 138254–138265.
[31] Z. Li, W. Shin, Y. Chen, et al., ACS Appl. Energy Mater. 2 (2019) 4053–4058.
[32] X. Wang, K. Han, D. Qin, et al., Nanoscale 9 (2017) 18216–18222.
[33] Y. Shen, C. Huang, Y. Li, et al., Electrochim. Acta 367 (2021) 137526–137534.
[34] F. Jing, T. Huang, G. Tao, et al., Electrochim. Acta 276 (2018) 207–213.
[35] Y. Bai, W. Fu, W. Chen, et al., J. Mater. Chem. A 7 (2019) 24454–24461.
[36] H. Wu, K. Wang, Y. Meng, et al., J. Mater. Chem. A 1 (2013) 6366–6372.
[37] W. Feng, N. Feng, W. Liu, et al., Adv. Energy Mater. 11 (2020) 2003215.
[38] W. Zhang, J. Ming, W. Zhao, et al., Adv. Funct. Mater. 29 (2019) 1903641.
[39] J. Zhao, X. Zou, Y. Zhu, et al., Adv. Funct. Mater. 26 (2016) 8103–8110.
[40] M. Jiang, N. Sun, R. Soomro, et al., J. Energy Chem. 55 (2021) 34–37.
[41] N. Sun, Q. Zhu, B. Anasori, et al., Adv. Funct. Mater. 29 (2019) 1906282.
[42] Q. Liu, F. Han, J. Zhou, et al., ACS Appl. Mater. Interfaces 12 (2020) 20838–20848.
[43] X. Wu, Y. Guo, J. Su, et al., Adv. Energy Mater. 3 (2013) 1155–1160.
[44] X. Wu, Z. Xing, Y. Hu, et al., Ionics 25 (2018) 2563–2574.
[45] Q. Zhu, X. Chang, N. Sun, et al., ACS Appl. Mater. Interfaces 11 (2019) 3107–3115.